frontiers | Frontiers in Chemistry

TYPE Original Research
PUBLISHED 11 July 2024
DOI 10.3389/fchem.2024.1405385

OPEN ACCESS

EDITED BY
Fadwa Odeh,
The University of Jordan, Jordan

REVIEWED BY
Kalpana Madgula (Garudadri), RiKarbon, Inc., United States
Buzuayehu Abebe,
Adama Science and Technology University, Ethiopia

*CORRESPONDENCE
Syed Ali Raza Naqvi,
draliraza@gcuf.edu.pk
Sadaf Ul Hassan,
sadafulhassan@cuilahore.edu.pk

RECEIVED 22 March 2024
ACCEPTED 11 June 2024
PUBLISHED 11 July 2024

CITATION
Rafique A, Amjad F, Janjua MRSA, Naqvi SAR, Hassan SU, Abdullah H, Nazir MS, Ali Z, Alshihri AA, Momenah MA, Mansour AA, Bajaber MA and Alalwiat AA (2024), Chia seed-mediated fabrication of ZnO/Ag/Ag_2O nanocomposites: structural, antioxidant, anticancer, and wound healing studies. *Front. Chem.* 12:1405385. doi: 10.3389/fchem.2024.1405385

Chia seed-mediated fabrication of ZnO/Ag/Ag_2O nanocomposites: structural, antioxidant, anticancer, and wound healing studies

Aisha Rafique[1], Fatima Amjad[2], Muhammad Ramzan Saeed Ashraf Janjua[1], Syed Ali Raza Naqvi[1]*, Sadaf Ul Hassan[2]*, Hanzla Abdullah[1], Muhammad Shahid Nazir[2], Zulfiqar Ali[2], Abdulaziz A. Alshihri[3], Maha Abdullah Momenah[4], Adel Abo Mansour[5], Majed A. Bajaber[6] and Ahlam A. Alalwiat[6]

[1]Department of Chemistry, Government College University Faisalabad, Faisalabad, Pakistan, [2]Department of Chemistry, COMSATS University Islamabad, Lahore, Pakistan, [3]Department of Radiological Sciences, College of Applied Medical Sciences, King Khalid University, Abha, Saudi Arabia, [4]Department of Biology, College of Science, Princess Nourah bint Abdulrahman University, Riyadh, Saudi Arabia, [5]Department of Clinical Laboratory Sciences, College of Applied Medical Sciences, King Khalid University, Abha, Saudi Arabia, [6]Chemistry Department, Faculty of Science, King Khalid University, Abha, Saudi Arabia

Plant extract-mediated fabrication of metal nanocomposites is used in cell proliferation inhibition and topical wound treatment, demonstrating significant effectiveness. *Salvia hispanica* L. (chia) seed extract (CE) is used as the reaction medium for the green fabrication of ecofriendly $ZnO_{(CE)}$ nanoparticles (NPs) and $Ag/Ag_2O_{(CE)}$ and $ZnO/Ag/Ag_2O_{(CE)}$ nanocomposites. The resultant nanoparticles and nanocomposite materials were characterized using UV–visible, Fourier-transform infrared (FTIR) spectroscopy, scanning electron microscopy (SEM), X-ray diffraction (XRD), and energy-dispersive X-ray (EDX) techniques. In the context of antioxidant studies, $ZnO/Ag/Ag_2O_{(CE)}$ exhibited 57% reducing power and 86% 2,2, diphenyl-1-picrylhydrazyl (DPPH) free radical scavenging. All three materials showed strong antibacterial activity against *Staphylococcus aureus* (*S. aureus*), *Escherichia coli* (*E.coli*), and *Bacillus subtilis* (*B. subtilis*) bacterial strains. Additionally, $ZnO_{(CE)}$, $Ag/Ag_2O_{(CE)}$, and $ZnO/Ag/Ag_2O_{(CE)}$ also revealed 64.47%, 42.56%, and 75.27% *in vitro* Michigan Cancer Foundation-7 (MCF7) cancer cell line inhibition, respectively, at a concentration of 100 µg/mL. Selectively, the most effective composite material, $ZnO/Ag/Ag_2O_{(CE)}$, was used to evaluate *in vivo* wound healing potential in rat models. The study revealed 96% wound closure in 10 days, which was quite rapid healing compared to wound healing using clinically available ointment. Therefore, in conclusion, the $ZnO/Ag/Ag_2O_{(CE)}$ nanocomposite material could be considered for further testing and formulation as a good anticancer and wound healing agent.

KEYWORDS

metallic nanoparticles and nanocomposite, green synthesis, antimicrobial *in vitro*, anticancer *in vitro*, wound healing *in vivo*

1 Introduction

The unique attributes of nanoparticles are augmented by their higher surface area/active mass-to-weight ratio, reactivity, and bioavailability. Their integration into nanocomposites and matrixes yielded nanomaterials with a unique set of physical, chemical, and biochemical properties, which resulted in intensive studies for a wide range of applications (Bilal et al., 2022). Over the last couple of decades, nanomaterials in the form of nanopowders, nanocomposites, nanofibers, etc., have been under extensive study to be used in potential applications, such as medical products and devices (Haleem et al., 2023), water treatment systems (Naseem and Durrani, 2021), air filters and air purifiers (Mahmoudi et al., 2023), polishing agents (Amir et al., 2022), catalysts (Patra et al., 2023), biosensors (Malik et al., 2023), food packaging and food protection films (Cushen et al., 2014), paints and varnish (Ganguli and Chaudhuri, 2021), and cosmetics (Włodarczyk and Kwarciak-Kozłowska, 2021). Among these applications, the design of innovative and multifunctional nanocomposites for anticancer, antimicrobial, and wound healing agents is of basic interest due to their life-saving nature. The most life-threatening disease is cancer, the most prevalent and leading cause of mortality in the world. Multiple options are in practice to create a barrier to its proliferation in the human body, but none has been perfected yet. Nanomaterials are engineered for this purpose (Nirmala et al., 2023). For example, the treatment of breast cancer involves loading doxorubicin into liposomes, followed by loading siRNA molecules onto solid lipid and other nanoparticles. These advancements were aimed at targeted therapy to enhance therapeutic efficacy (Senapati et al., 2018). Photothermal therapy (PTT), using gold and silver nanoparticles, is being exercised to destroy cancer cells and stimulate immune responses (Borzęcka et al., 2022). Moreover, as drug delivery systems (DDSs), nanoparticles play a pivotal role in improving the therapeutic efficacy of anticancer treatment and reducing the cytotoxic effect (Sharma et al., 2023). Bacterial infection is a global burden due to its life-threatening outbreaks. A long history of microbial infection treatment is associated with antibiotics, but according to the reported data and experienced clinicians, sooner or later, bacterial resistance becomes a hallmark of the use of antibiotics, which reduces their efficacy significantly. Nanomaterials paralyze and kill bacteria effectively and also eliminate the chance of bacterial resistance. These potential properties intensify attempts to develop antibacterial nanomaterials to treat different infectious ailments, such as deep-seated infections and wound healing (Gupta et al., 2019; Nandhini et al., 2024). The use of antibacterial compounds is not only limited to the *in vivo* treatment of bacterial infections but is also required for disinfecting healthcare instruments, especially surgical tools. Reported data advocate that gold nanoparticles and quantum dots, using infrared light, play a vital role in disinfecting the instruments from bacteria (Haleem et al., 2023).

Wounds are injuries to the skin tissues caused by external stimuli or trauma, categorized as acute and chronic wounds based on their healing period. Acute wounds take few weeks to heal, while chronic wounds may take several months. Contamination, colonization, and infection are the three main stages in the wound infection continuum (Li et al., 2021). Wound contamination represents the microbes in non-replicating form in an open wound. This stage does not affect the normal inflammatory response or wound healing process. Untreated microbes start replicating into colonies, which further damages the tissue and partially inactivates the inflammatory response. Further migration and replication of microbes deep into the wound bed result in an immune reaction with the characteristics of infection (acute state) (Swanson et al., 2015). The production of the glycocalyx (biofilm) by some microbes at the wound site leads to the development of a protective layer, which makes the wound hard to detect and treat (chronic state) (Malone et al., 2017). Further progression may lead to systemic complications (cellulitis, osteomyelitis, and septicemia) from topical wounds (Li et al., 2021). Chronic wounds affect approximately 20 million people globally, with an economic burden of approximately $31 billion per year for treatment and management (Järbrink et al., 2017; Nussbaum et al., 2018).

The wound healing process is an intricate interaction among wound cells, the components of the extracellular matrix, and biochemical signal pathways. Commonly exercised traditional wound healing treatments are a slow process, which is associated with some typical limitations such as sluggish tissue regeneration, long-term persistence of wound infections, and poor wound closure. This hampers the wound healing process seriously. Nanotechnology has created new research opportunities in the field of wound healing strategies and has made significant advances in cancer therapy and wound healing (Nandhini et al., 2024). Metallic nanoparticles (NPs), such as silver (Ag), gold (Au), and zinc (Zn), have been reported to have promising bactericidal properties and low cytotoxicity, which make them useful for wound healing (Rajendran et al., 2018). Ag NPs aid in the healing of superficial wounds (Solanki et al., 2023) and are often combined with other metals, particularly Au and Zn, to boost their antibacterial potential. Physical and chemical methods of NP synthesis are gradually being replaced by ecofriendly green synthesis methods because of their multiple demerits, such as the release of toxic and harmful chemicals, consumption of a large amount of energy, and use of complex synthesis conditions and equipment (Ying et al., 2022). The green synthesis of ZnO NP/silica gel dressings using *Aloe barbadensis* leaf extract was found effective in healing mouse wounds (Batool et al., 2020). The blend of Ag and Zn NPs has also been used in wound healing, such as the 1% Ag–ZnO/silver oxide (AgO) nanocomposites currently being investigated for the treatment of topical wounds (de Moura et al., 2022), chitosan dressings loaded with Ag and Zn NPs (chitosan/AgO/ZnO) (Li et al., 2010), and chitosan/polyethylene glycol/ZnO/Ag (chitosan/PEG/ZnO/Ag) nanocomposite dressings (Liu and Kim, 2012). Hydrogels containing Ag@ZnO core–shell nanocomposites synthesized from the leaf extract of *Hibiscus sabdariffa* were used for wound healing in a mouse model (Malone et al., 2017).

Salvia hispanica L. is a flowering plant belonging to the mint family (Lamiaceae) native to central and southern Mexico. The seeds obtained from this plant are commonly termed chia seeds, which possess a great deal of nutritional and medicinal value. Chia seeds are a potential source for synthesizing nanomaterials as they are readily available, inexpensive, and can easily be processed into different forms (such as gel, powder, and liquid). This easy processability is the main reason for using chia seeds as a source for nanoparticle synthesis. Chia seeds are made up of proteins,

lipids, polysaccharides, some phytochemicals, flavonoids, and phenolic compounds. These flavonoids and phenolic acids act as great reducing agents and stabilizing agents for the nanoparticles. These compounds also provide great antioxidant properties to the nanomaterials; hence, they are potential antibacterial and antioxidant materials. Compounds like alpha-linolenic acid reduce inflammation and can inhibit cancer cell growth, and flavonoids and chlorogenic acid help neutralize harmful free radicals in the body, which can protect the body from bacterial attacks, reduce inflammation, and inhibit cancer cell growth. Phytochemicals like quercetin, kaempferol, and caffeic acid have the chemical ability to interfere with cancer cell proliferation, induce apoptosis (programmed cell death), and inhibit angiogenesis (the formation of new blood vessels that supply tumors), hence contributing to anticancer activity. The chemical composition of chia seeds allows easy modification through simple chemical or enzymatic treatments, further expanding their potential applications in nanoparticle synthesis (Reyes-Caudillo et al., 2008). The use of dark chia seed extract (CE) in the synthesis of Ag NPs boosted their antimicrobial activities (Hernández-Morales et al., 2019). The aim of this study is to synthesize $ZnO_{(CE)}$ NPs, $Ag/Ag_2O_{(CE)}$, and $ZnO/Ag/Ag_2O_{(CE)}$ nanocomposites by using the aqueous extract of chia seeds as a reducing and stabilizing reagent for the investigation of anticancer, antibacterial, and wound healing potential.

2 Materials and methods

2.1 Chemicals

Silver nitrate ($AgNO_3$), zinc nitrate hexahydrate ($Zn(NO_3)_2.6H_2O$), sodium hydroxide (NaOH), sodium phosphate, potassium ferricyanide, trichloroacetic acid, ferric chloride, ascorbic acid, 2,2, diphenyl-1-picrylhydrazyl (DPPH), methanol, 3-(4,5-dimethylthiazol-2-yl)-2,5-diphenyl-2H-tetrazolium bromide (MTT), dimethyl sulfoxide, and Mueller Hinton agar (MHA) were obtained from Sigma-Aldrich and used without further purification. Chia seeds were obtained from the local market. All the solutions were prepared in double-distilled deionized water.

2.2 Preparation of the chia seed extract

Chia seeds (9.6 g) were cleaned three times using distilled water and dried at room temperature. After drying, the chia seeds were heated in 100 mL of distilled water for 30 min and immediately filtrated using a nylon-fiber sieve. The CE was stored in a refrigerator at 5°C and used for NP synthesis a day after its preparation for the best antimicrobial results (Hernández-Morales et al., 2019).

2.3 Synthesis of ZnO NPs

The CE (30 mL) was heated at 60°C, followed by the addition of 1.33 g of $Zn(NO_3)_2.6H_2O$ (0.15 M) and agitated for at least 4 h. The solution color changed from transparent to light brown, indicating the formation of precipitates. The solution was cooled to room temperature and then centrifuged at 4,000 rpm for 20 min. The prepared nanoparticles were rinsed repeatedly in distilled water to remove any unreacted material. The material was dried at 80°C for 6 h and then calcinated at 500°C for 4 h (Sorbiun et al., 2018).

2.4 Synthesis of the Ag/Ag_2O nanocomposite

$Ag/Ag_2O_{(CE)}$ was synthesized by adding 0.8491 g $AgNO_3$ to 20 mL deionized water and mixing well to form a uniform solution (0.25 M), followed by the addition of 1.6 mL CE. The mixture was stirred vigorously for 15 min. The precipitates turned the color of the solution from transparent to light yellow. Further overnight stirring at room temperature was carried out to obtain AgO NPs. The resultant mixture was centrifuged at 4,000 rpm for 10 min. The prepared precipitates were separated, dried at 80°C, and then calcinated at 300°C for 2 h. The resulting brown precipitates indicated the successful synthesis of $Ag/Ag_2O_{(CE)}$ (Hernández-Morales et al., 2019).

2.5 Synthesis of the $ZnO/Ag/Ag_2O$ nanocomposite

The $ZnO/Ag/Ag_2O$ nanocomposite was prepared using a co-precipitation method with slight modifications (Hernández-Morales et al., 2019). The nanocomposite was synthesized by the addition of $AgNO_3$ (0.212 g~0.025 M [0.0012 mol]) and $Zn(NO_3)_2.6H_2O$ (0.376 g~0.025 M [0.0012 mol]) to 50 mL of distilled water. The components were mixed well to create a homogeneous solution. Then, 1.6 mL of CE was added dropwise under vigorous stirring for 15 min at ambient temperature. The change in the color of the solution from transparent to brown was an indication of precipitate formation. Overnight stirring of the solution resulted in brown precipitates settling at the bottom of the beaker. The mixture was centrifuged at 4,000 rpm for 10 min, followed by the collection of precipitates, drying at 80°C for 6 h, and then calcination at 400°C for 4 h. $ZnO/Ag/Ag_2O_{(CE)}$ nanocomposites were consequently obtained in the form of brown powder. The visual analysis of the final nanomaterials synthesized is shown in Supplementary Figure S1.

2.6 Characterizations

A UV–visible spectrophotometer (Shimadzu UV-2550 Spectrophotometer), Fourier-transform infrared (FTIR) spectrophotometer (Nicolet Magna 550 Spectrophotometer), scanning electron microscope, powder X-ray diffractometer, and energy-dispersive X-ray (EDX) spectrophotometer were used to characterize $ZnO_{(CE)}$ NPs and $Ag/Ag_2O_{(CE)}$ and $ZnO/Ag/Ag_2O_{(CE)}$ composites in order to identify their physical features. The UV–visible spectra in the range of 200–800 nm were recorded. The FTIR spectrophotometer covering a wave number range of 650–4,000 cm^{-1} was utilized to determine the functional groups found in $ZnO_{(CE)}$ NPs and $Ag/Ag_2O_{(CE)}$ and $ZnO/Ag/Ag_2O_{(CE)}$ nanocomposites. SEM investigated the appearance and structure of nanoparticles and nanocomposites. XRD patterns were recorded

using a PANalytical X'Pert (Naseem and Durrani, 2021) material research diffractometer with CuKα radiation to determine sample phases in the range of 10°–80°.

2.7 Antioxidant study

The antioxidant potential of the synthesized NPs and nanocomposites was determined using the most commonly adopted methods, such as reducing power and DPPH free radical scavenging assays.

2.7.1 Reducing power assay

The antioxidant activity of $ZnO_{(CE)}$, $Ag/Ag_2O_{(CE)}$, and $ZnO/Ag/Ag_2O_{(CE)}$ was determined according to a method described previously (Soni and Dhiman, 2017). In brief, 2.5 mL of different concentrations (62.5 µg/mL, 125 µg/mL, 250 µg/mL, 500 µg/mL, and 1,000 µg/mL) of the sample ($ZnO_{(CE)}$ or $Ag/Ag_2O_{(CE)}$ or $ZnO/Ag/Ag_2O_{(CE)}$) was added separately to 2.5 mL of 200 mmol/L sodium phosphate (pH 6.6), which was then mixed with 2.5 mL of the potassium ferricyanide solution. The mixture was then incubated at 50 C for 20 min, followed by the addition of 2.5 mL of 10% trichloroacetic acid (w/v), and centrifuged at 650 rpm for 10 min. After centrifugation, 5 mL of the supernatant was mixed with 5 mL of distilled water and 1 mL of 0.1% ferric chloride. The absorbance of this solution was measured at 700 nm compared to ascorbic acid used as the standard. Higher absorbance yielded a higher reducing potential.

2.7.2 DPPH free radical scavenging assay

The (DPPH free radical assay was carried out to assess the radical scavenging activity of the antioxidant component using a previously reported protocol (Al-Shmgani et al., 2016). In brief, a $ZnO_{(CE)}$, $Ag/Ag_2O_{(CE)}$, or $ZnO/Ag/Ag_2O_{(CE)}$ sample methanol solution of different concentrations (125 µg–1,000 µg/mL) was mixed with 4 mL of the 0.2 mM methanol solution of DPPH free radical. After 30 min of incubation at room temperature, the absorbance was recorded at 517 nm. The scavenging activity was measured using Eq 1:

$$\%\ \text{of inhibition} = \left(A_{blank} - A_{Sample}\right)/A_{blank} * 100, \quad (1)$$

where A_{blank} is the absorbance of the DPPH solution and A_{sample} is the absorbance of the sample solution. The lower the absorbance, the higher the DPPH radical scavenging activity.

2.8 Antibacterial potential study

The antimicrobial activity of $ZnO_{(CE)}$ NPs and $Ag/Ag_2O_{(CE)}$ and $ZnO/Ag/Ag_2O_{(CE)}$ nanocomposites was investigated using the well diffusion method with slight modifications, as previously reported (Al-Shmgani et al., 2016). The antibacterial activity was assessed against three bacterial strains: *S. aureus*, *B. subtilis*, and *E. coli*. An agar solution containing 3.8 gMH of agar was prepared and sterilized in an autoclave. The sterilized media were then transferred to Petri dishes, and bacterial cultures were spread on the solid medium surface. A stock solution of nanocomposites was prepared at various concentrations (3 mg/mL, 1.5 mg/mL, 0.750 mg/mL, and 0.375 mg/mL). DMSO and CFR 30 of 30 µg/mL were used as the negative and positive controls, respectively. Six wells were punctured in each Petri plate, 40 ppm solution from each dilution was inoculated into every Petri dish, and a CFR 30 disc was placed in the center. These Petri dishes were incubated at 37°C for 24 h. After 24 h, the nanocomposites inhibited the growth of the bacterial cultures, and the diameter of the zone of inhibition (ZOI, mm) was measured against each organism. Triplicate measurements were taken to ensure the accuracy and reliability of the results.

2.9 Anticancer activity

Using a slightly altered MTT assay developed by Bio Basic Inc. (Canada), the cytotoxicity of $ZnO_{(CE)}$ NPs and $Ag/Ag_2O_{(CE)}$ and $ZnO/Ag/Ag_2O_{(CE)}$ nanocomposites was evaluated using the breast cancer cell line MCF7 provided by the American Type Culture Collection (ATCC) center (Hashem and El-Sayyad, 2023). The viability and inhibition percentages were determined using the following Eqs 2, 3, respectively:

$$Viability\% = \frac{Sample\ optical\ density}{Control\ optical\ density} \times 100 \quad (2)$$

$$\%Inhibition = 100 - Viability\% \quad (3)$$

2.10 Wound healing *in vivo* studies

The Department of Pharmaceutics, Government College University Faisalabad, Pakistan, approved the experimental methods for analyzing wound healing. The four mice used in the experiment were categorized into two groups, each with a pair of mice. Group I was designated as the control group, and group II was treated with $ZnO/Ag/Ag_2O_{(CE)}$. Under anesthesia with chloroform, a full-thickness excision wound measuring 6 mm was made after shaving the dorsal side hair of the mice using a sterile surgical blade. The mice in the treatment group were given 1 mL of synthetic $ZnO/Ag/Ag_2O_{(CE)}$ (2 mM) in the form of niosomes, whereas the mice in the control group were given 1 mL of standard saline. These ingredients were mixed into a 2 × 2-cm^2 dressing, which was then placed on the wound bed. For 10 days, this application was done once every day. The contraction of the wound tissue was observed at intervals of 0, 2, 4, 6, 8, and 10 days to gauge the degree of wound healing. Additionally, on the specified days, pictures of the wounds in the control and treated mice were taken and compared (Al-Shmgani et al., 2016).

3 Results and discussion

3.1 FTIR studies

FTIR analysis identified the functional groups in the $ZnO_{(CE)}$ NPs and $Ag/Ag_2O_{(CE)}$, and $ZnO/Ag/Ag_2O_{(CE)}$ nanocomposites, as shown in Figure 1, with spectral ranges from 4,000 to 600 cm^{-1}. Specifically, the band within 3,483.2–3,286.0 cm^{-1} is due to O-H group stretching vibrations from phytochemicals like polyphenols, alkaloids, and

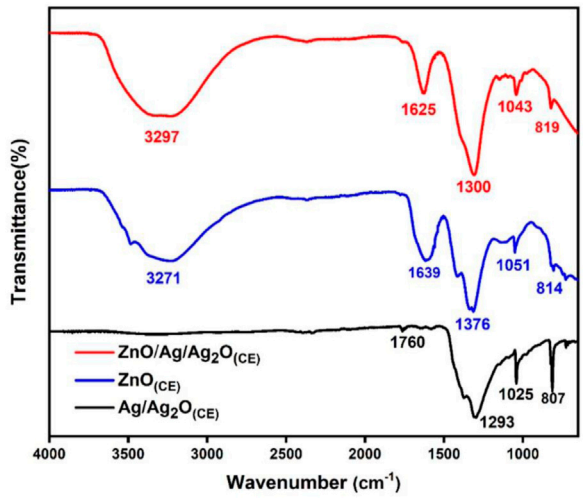

FIGURE 1
FTIR spectra of $ZnO_{(CE)}$, $Ag/Ag_2O_{(CE)}$, $ZnO/Ag/Ag_2O_{(CE)}$.

flavonoids in the chia seed extract, confirming the existence of diverse encapsulated and reducing bioactive molecules in the extract (Hernández-Morales et al., 2019). In the case of $Ag/Ag_2O_{(CE)}$, the faint band observed in the AgO spectrum at approximately 3,238 cm^{-1} can be allocated to the stretching of the C–H bonds in the aldehyde molecule. Various absorbent bands at 1,760 cm^{-1}, 1,373 cm^{-1}, 1,293 cm^{-1}, and 1,070–1,000 cm^{-1} are due to C=C bond vibrations associated with stretching (Laouini et al., 2021), the presence of C-O (Sobhani-Nasab and Behpour, 2015) and C=O stretching vibrations due to carbonyl and carboxylate groups (Jaiswal et al., 2022), and CH_2O stretching or bending vibrational bands (Chen et al., 2014). Furthermore, C-H bending was identified as the cause of the band observed at 807 cm^{-1} (Barwant et al., 2022). The absorption range observed in $ZnO_{(CE)}$ at 3,271 cm^{-1}, 1,638.7 cm^{-1}, 1,376.2 cm^{-1}, 1,050.9 cm^{-1}, and 814 cm^{-1} is linked to the O-H stretching vibrations of alcoholic and carboxylic groups, C=C bonding in alkene, C-H stretching of the methyl group, C-O bonding in polysaccharides (Zafar et al., 2021), and the O-H functional group (Sorbiun et al., 2018). The FTIR spectrum of $ZnO/Ag/Ag_2O_{(CE)}$ indicates the existence of a strong band at approximately 3,296 cm^{-1} linked to the vibratory stretching of the hydrogen-bonded O-H group, indicating that the water molecules are captured by the samples (Ding et al., 2019). The bands observed at 1,625 cm^{-1} and 1,524 cm^{-1} indicated the C=C stretching vibrations (Thatikayala et al., 2020) and the N-O stretching band, respectively. Furthermore, bands between 1,300 and 1,043 cm^{-1} were detected, attributed to the O-H bending and CO-O-CO stretching of bonds. C = C bending vibrations of unsaturated compounds in the seed extract were observed at 819 cm^{-1}. In the case of $ZnO/Ag/Ag_2O_{(CE)}$, a distinct peak was observed within the 1,094–821 cm^{-1} range, corresponding to the combined absorptions of Zn-O and Ag-O bonds.

3.2 XRD studies

The X-ray diffraction spectrum of $Ag/Ag_2O_{(CE)}$ is shown in Supplementary Figure S2. Several diffraction patterns were observed in the face-centered cubic structure at 38.1, 44.3, and 64.6 corresponding to the metallic Ag (111), (200), and (220), respectively (JCPDS card no. 04-0783) (Elyamny et al., 2021). Changes required. Peaks at 32.7°, 38.06°, 54.8°, and 65.6° were assigned to cubic phase Ag_2O diffraction planes (111), (200), (220), and (311) (JCPDS card no. 41-1104) (Sophia et al., 2020). The average size of the Ag/Ag_2O nanoparticles was calculated using Scherrer's equation (Eq. 4) and the full breadth at half-maximum (FWHM) of the diffraction patterns.

$$D = \frac{K\lambda}{\beta \cos \theta}. \quad (4)$$

Here, D is the crystalline size of the nanoparticles, K denotes a constant of 0.94, λ is the wavelength of radiation (1.54056 Å for CuKα radiation), β is the peak breadth at half-maximum intensity, and Θ is the peak position. Thus, the average size of the green synthesized $Ag/Ag_2O_{(CE)}$ nanoparticles was 46.6 nm. The XRD pattern of the green synthesized ZnO nanoparticles, as shown in Supplementary Figure S2, indicates the crystalline structure of the synthesized nanoparticles. The sharp diffraction bands were observed at 2Θ values: 31.68, 34.34, 36.02, 47.51, 56.26, 62.67, 67.1 68.18, 69.73, 72.7, and 77.7 of (100), (002), (101), (102), (110), (103), (200), (112), (201), (004), and (202) planes, respectively, which confirms the hexagonal wurtzite structure (JCPDS no. 75-1526) of the synthesized nanoparticles (Althubiti et al., 2023). Thus, the average dimension of green synthesized ZnO nanoparticles is estimated to be 16.15 nm.

The XRD spectra of the $ZnO/Ag/Ag_2O_{(CE)}$ nanocomposite obtained (Figure 2A) were confirmed against the standards of Ag, Ag_2O, and ZnO. The diffraction lines located at 38.1 (111), 44.28 (200), and 64.6 (220) verified the presence of Ag in the $ZnO/Ag/Ag_2O$ composite (JCPDS card no. 04-0783) (Umukoro et al., 2016). Peaks at 32.1 (111), 38.1 (200), 55.1 (220), and 65.4 (311) can be attributed to the crystalline plane of Ag_2O (JCPDS card no. 41-1104). Thus, it is validated that Ag and Ag_2O exist together in $ZnO/Ag/Ag_2O$ (Umukoro et al., 2016). The remaining characteristic peaks at 31.8°, 34.4°, 36.3°, 47.5°, 56.6°, 62.9°, 67.9°, 68.7°, and 69.1° match (100), (002), (101), (102), (110), (103), (200), (112), and (201) crystalline orientations of ZnO (Ding et al., 2019). The suggested average particle size of the nanocomposite was 22.42 nm. The doping of ZnO into Ag/Ag_2O induces alterations in peak intensity and diffraction angle in the XRD patterns depicted in Figure 2B. This doping may introduce new phases into the host material, leading to reduced peak intensity as crystal planes undergo transformation. Additionally, a minor shift toward higher angles occurs, which is attributed to the expansion of host lattice parameters in the final composite $ZnO/Ag/Ag_2O$ (Hosseini et al., 2015; Pandi et al., 2023).

3.3 UV–visible studies

The UV–visible spectra of chia seed mucilage, $ZnO_{(CE)}$ NPs, and $Ag/Ag_2O_{(CE)}$ and $AgO.ZnO_{(CE)}$ nanocomposites are shown in Figure 3A. The peak observed at 315 nm shows the interaction of phenols, flavonoids, and alkaloids in the chia seed mucilage. The chia seed mucilage peak is used as the standard. $Ag/Ag_2O_{(CE)}$

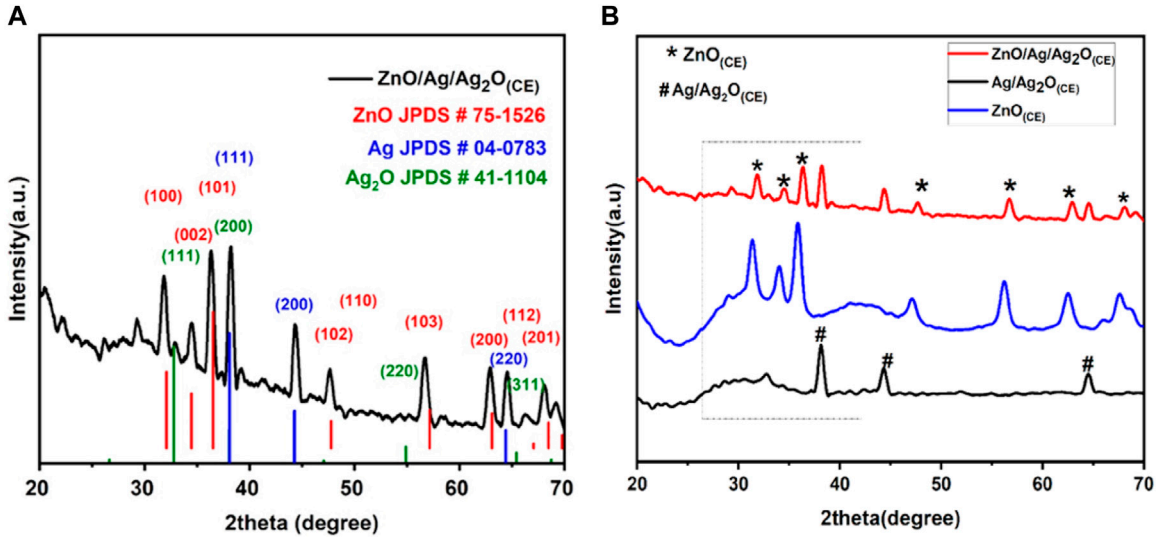

FIGURE 2
(A) XRD spectra of $ZnO/Ag/Ag_2O_{(CE)}$. **(B)** Stacked XRD graphs of $ZnO_{(CE)}$, $Ag/Ag_2O_{(CE)}$, and $ZnO/Ag/Ag_2O_{(CE)}$.

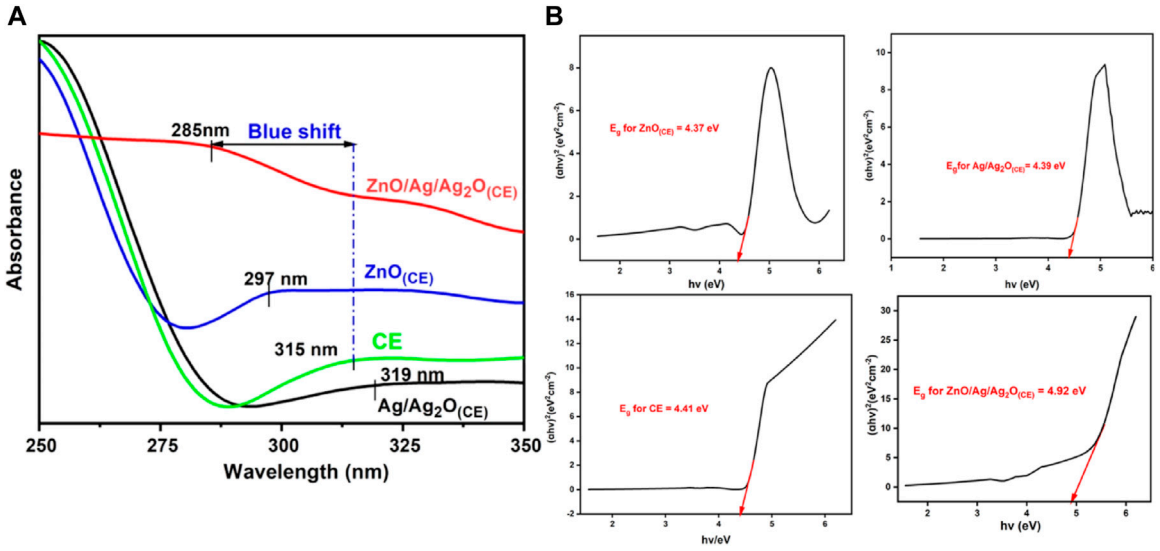

FIGURE 3
(A) UV–visible spectra of chia seed extract, $ZnO_{(CE)}$, $Ag/Ag_2O_{(CE)}$, and $ZnO/Ag/Ag_2O_{(CE)}$. **(B)** Tauc's plot analysis for band gap energy calculations of the prepared nanocomposites.

shows a peak at 319 nm, indicating the conjugation of AgO and the chia seed due to the appearance of a redshift, while the $ZnO_{(CE)}$ peak was observed at 297 nm, showing a blue shift compared to the chia seed mucilage. The peak at 285 nm exhibited by $ZnO/Ag/Ag_2O_{(CE)}$ showed a higher blue shift of 30 nm compared to the chia seed mucilage. This optical property was also supported by calculating the Tauc plots for the $Ag/Ag_2O_{(CE)}$, $ZnO_{(CE)}$, chia seed extract, and final $ZnO/Ag/Ag_2O_{(CE)}$ composite (Figure 3B). The band gap energies of $Ag/Ag_2O_{(CE)}$, $ZnO_{(CE)}$, chia seed extract, and $ZnO/Ag/Ag_2O_{(CE)}$ were calculated as 4.39, 4.38, 4.41, and 4.92 eV, respectively. This increase in the band gap energy of the final composite compared to the $Ag/Ag_2O_{(CE)}$, $ZnO_{(CE)}$, and chia seed extract also confirms the predicted blue shift. This increase also justified the infiltration of the dopants in the final composite.

3.4 SEM analysis

SEM is used to study the fabrication of the $Ag/Ag_2O_{(CE)}$ nanocomposite (Figure 4A) and shows a particle-like heterostructure; there is no obvious difference between the

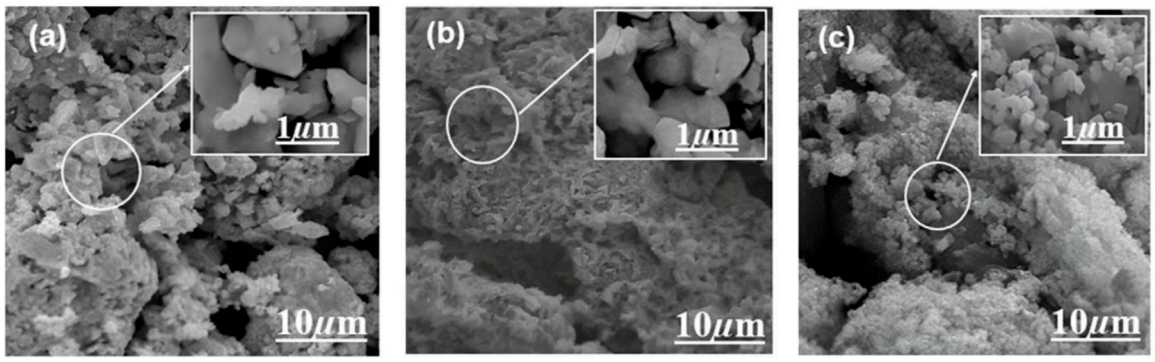

FIGURE 4
SEM images of **(A)** $Ag/Ag_2O_{(CE)}$, **(B)** $ZnO_{(CE)}$, and **(C)** $ZnO/Ag/Ag_2O_{(CE)}$.

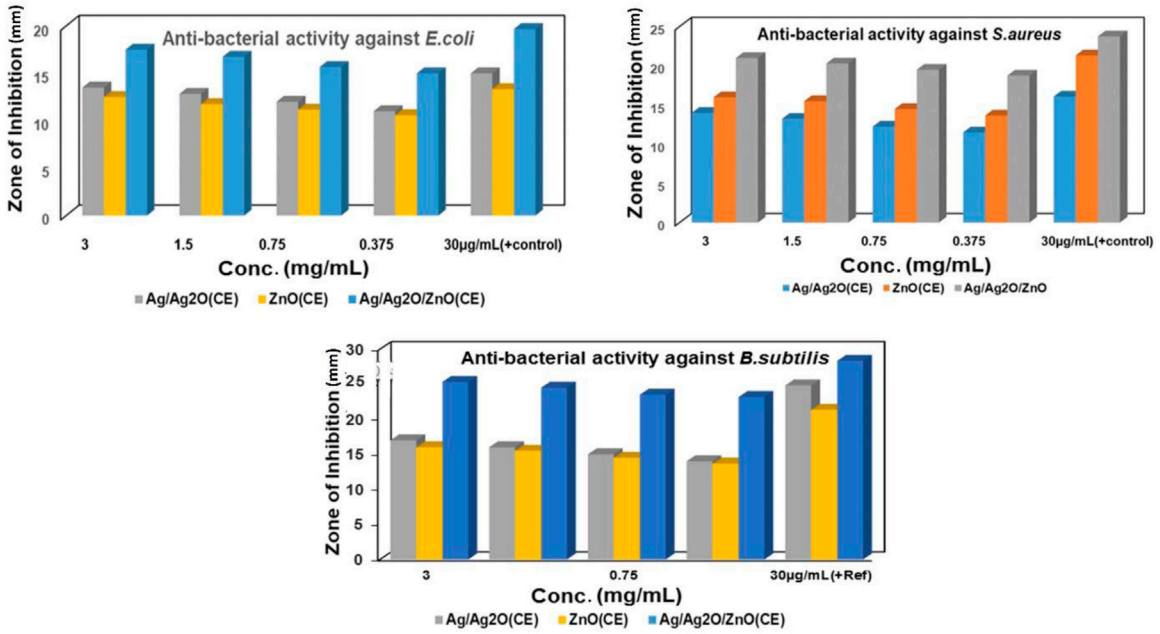

FIGURE 5
Antibacterial activity of $ZnO_{(CE)}$, $Ag/Ag_2O_{(CE)}$, and $ZnO/Ag/Ag_2O_{(CE)}$ against *B. subtilis*.

morphology and size of Ag and Ag/Ag_2O (Yang et al., 2016). Figure 4B shows the SEM images of $ZnO_{(CE)}$ NPs at a lower resolution; it shows that particles are agglomerated and complete separation has probably not happened, while a higher magnification image shows irregularly shaped nanoparticles (Mohan and Renjanadevi, 2016). Figure 4C shows a spherical-shaped nanocomposite of $ZnO/Ag/Ag_2O_{(CE)}$ (Umukoro et al., 2016). EDX analysis also showed the presence of silver oxide, zinc oxide, and the $ZnO/Ag/Ag_2O$ composite (Supplementary Figure S3).

3.5 Antibacterial studies

Bio-synthesized ZnO NPs and Ag/Ag_2O and $ZnO/Ag/Ag_2O$ nanocomposites were evaluated for their antibacterial activity toward *S. aureus*, *B. subtilis*, and *E. coli* using the well diffusion approach, as shown in Supplementary Figure S4. It was observed that microbial growth of 3 mg/mL of NPs showed the highest diameter of the zone of inhibition against each microorganism. The maximum zone of inhibition was shown by $Ag/Ag_2O_{(CE)}$ at 3 mg/mL against *B. subtilis*, at 17 mm and 14 mm toward *S. aureus*, and 13.5 mm against *E. coli*, while $ZnO_{(CE)}$ demonstrated the maximum ZOI at 16 mm against *B. subtilis*, 14 mm against *S. aureus*, and 12.5 mm against *E. coli*. The ZOI was shown by $ZnO/Ag/Ag_2O_{(CE)}$ at 25.3 mm against *B. subtilis*, 21 mm against *S. aureus*, and 17.5 mm against *E. coli* at 3 mg/mL.

The negative control showed no ZOI, and the positive control showed the highest inhibition against *B. subtilis*. Among these NPs and nanocomposites, $ZnO/Ag/Ag_2O_{(CE)}$ exhibited the maximum zone of inhibition against *B. subtilis* at 25 mm. ZnO is toxic to

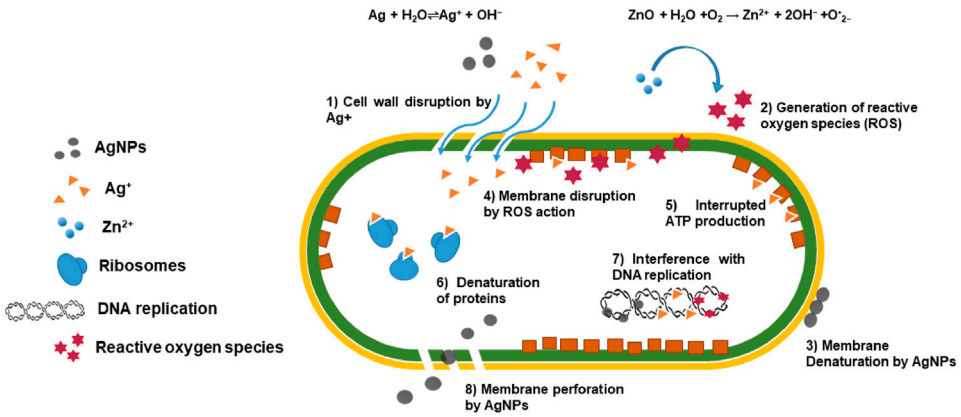

FIGURE 6
Antibacterial action of the prepared ZnO/Ag/Ag_2O nanocomposites.

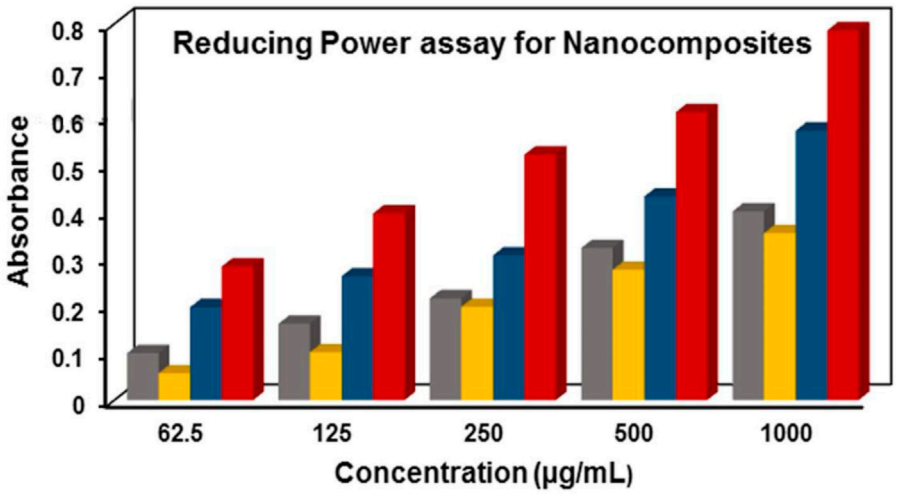

FIGURE 7
Reducing power assay for $ZnO_{(CE)}$ (yellow), $Ag/Ag_2O_{(CE)}$ (gray), $ZnO/Ag/Ag_2O_{(CE)}$ (blue) and ascorbic $acid_{(Ref)}$ (red).

bacteria and has antibacterial properties against resilient species (Bilal et al., 2022). Previous studies showed that growth inhibition increased with increasing NP content in wells, and a similar case was observed in this study (Lawrence, 2015). Depending on the size and concentration of the NPs, the inhibitory zone dimension differed against various bacteria. Antimicrobial activity against *S. aureus*, *E. coli*, and *B. subtilis* is shown in Figure 5.

The general antibacterial action of the prepared nanocomposites occurs when ZnO and Ag/Ag_2O nanoparticles work synergistically for their antibacterial activity. ZnO nanoparticles generate reactive oxygen species (ROS), such as superoxide radicals ($O\bullet^{2-}$), hydroxyl radicals ($OH\bullet$), and singlet oxygen, under light irradiation or in an aerobic environment. The reaction can be represented as

$$ZnO + H_2O + O_2 \rightarrow Zn^{2+} + 2OH - + O\bullet^{2-}.$$

These ROS can induce oxidative stress in bacterial cells, causing damage to lipids, proteins, and DNA, ultimately causing cell death. Similarly, Ag/Ag_2O nanoparticles release silver ions (Ag+) in the presence of aqueous media or in contact with bacterial cell membranes. The reaction can be represented as

$$Ag + H_2O \rightleftharpoons Ag + + OH - .$$

Silver ions disrupt bacterial cell membrane integrity, interfere with cell division, and inhibit enzymatic activity crucial for bacterial survival. This combined action of ROS generated by ZnO and silver ions released from Ag/Ag_2O nanoparticles results in a synergistic antibacterial effect. ROS cause oxidative damage to bacterial cells, making them more susceptible to the antimicrobial action of silver ions. Additionally, silver ions can enhance ROS generation by ZnO through redox reactions, further amplifying the antibacterial activity. The cumulative effects of ROS-induced oxidative stress and silver ion toxicity lead to irreversible damage to bacterial cells. This antibacterial action is shown in Figure 6.

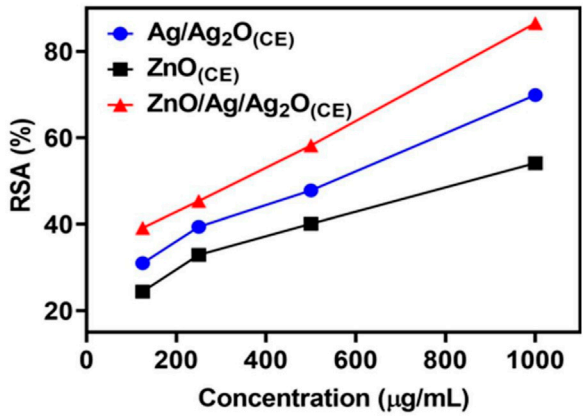

FIGURE 8
DPPH radical scavenging activity of $Ag/Ag_2O_{(CE)}$, $ZnO_{(CE)}$, and $ZnO/Ag/Ag_2O_{(CE)}$.

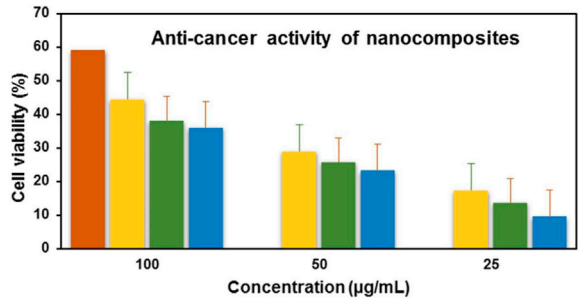

FIGURE 9
Anticancer activity of doxorubicin(+) (red), $ZnO_{(CE)}$ (green), $Ag/Ag_2O_{(CE)}$ (blue), $ZnO/Ag/Ag_2O$ (yellow).

3.6 Antioxidant activities

3.6.1 Reducing power activity

Free radicals which are highly reactive molecules can be neutralized by obtaining electrons from antioxidants. Antioxidants stabilize these free radicals by donating electrons, known as their reducing power. This reducing power is utilized in the chemical reaction where Fe^{+3}/ferrocyanide complex is converted to its ferrous(Fe^{+2}) form through direct electron donation (Karthick et al., 2012). The product was measured at 700 nm after a strong Prussian blue complex was formed. The reducing capacity of $Ag/Ag_2O_{(CE)}$ exhibited absorbance values of 0.099, 0.162, 0.216, 0.323, and 0.401, whereas $ZnO_{(CE)}$ displayed absorbance values of 0.0571, 0.1016, 0.198, 0.277, and 0.355. The $ZnO/Ag/Ag_2O_{(CE)}$ nanocomposite exhibited absorbance values of 0.197, 0.263, 0.307, 0.433, and 0.573, while the standard ascorbic acid exhibited optical density values of 0.284, 0.397, 0.522, 0.612, and 0.786, as shown in Figure 7. Increased absorbance of the reaction mixture or concentration-dependent reducing power was demonstrated by the nanocomposites. However, their reducing power was not as powerful as that of ascorbic acid (standard), which demonstrated the highest reducing activity. Reactive radicals can be reduced to more stable and non-reactive forms by receiving electrons from antioxidant substances (Gülçın et al., 2003). The outcomes from such investigations indicated that the synthesized $ZnO/Ag/Ag_2O_{(CE)}$ possessed higher antioxidant activity than $Ag/Ag_2O_{(CE)}$ and $ZnO_{(CE)}$. It was found that absorbance increased with the sample concentration. Higher reaction mixture absorbance suggests higher reduction efficiency.

3.6.2 DPPH free radical scavenging study

The free radical scavenging activity of the $ZnO_{(CE)}$ NPs and $Ag/Ag_2O_{(CE)}$ and $ZnO/Ag/Ag_2O_{(CE)}$ nanocomposites was evaluated using the DPPH technique. The analysis was carried out thrice. At the maximum concentration of 1,000 µg/mL, the synthesized $Ag/Ag_2O_{(CE)}$ had better antioxidant activity of 69.91%, whereas $ZnO_{(CE)}$ exhibited higher DPPH activity of 52.138% at 1,000 µg/mL. $ZnO/Ag/Ag_2O_{(CE)}$ showed the highest radical scavenging activity of 86.554% at 1,000 µg/mL (Aththanayaka et al., 2023). Antioxidant activity increased with the concentration of the tested samples in the DPPH assay (Awan et al., 2023). Thus, the antioxidant activity of $ZnO/Ag/Ag_2O_{(CE)}$ was higher than that of $Ag/Ag_2O_{(CE)}$ NPs and $ZnO_{(CE)}$, which was significant (Figure 8).

3.7 Anticancer activity

Anticancer analysis results revealed that $ZnO_{(CE)}$ NPs and $Ag/Ag_2O_{(CE)}$ and $ZnO/Ag/Ag_2O_{(CE)}$ nanocomposites exhibited anticancer activity against MCF7 breast cancer cells, with IC_{50} values of 100.24, 100.26, and 100.23, respectively (Narayan et al., 2010). The anticancer activity of $ZnO_{(CE)}$, $Ag/Ag_2O_{(CE)}$, and $Zn/Ag/Ag_2O_{(CE)}$ toward MCF7 at a concentration of 100 µg/mL was 64.47%, 42.56%, and 75.27%, respectively, as shown in Figure 9. Metal oxide nanoparticles (ZnO and Ag/Ag_2O) and nanocomposites ($ZnO/Ag/Ag_2O$) generate free radicals, which give rise to ROS. The ROS induce oxidative stress in cancer cells by disrupting the cellular metabolic pathways and damaging DNA, proteins, and lipids, leading to apoptosis. In the $ZnO/Ag/Ag_2O$ nanocomposite, zinc and silver free radicals interfere with the mitochondrial protease, resulting in apoptosis through caspase activation, and inhibit the cell cycle to stop further cancer proliferation (Roshani et al., 2023). The proposed anticancer mechanism of the $ZnO/Ag/Ag_2O$ nanocomposite is shown in Figure 10.

3.8 *In vivo* wound healing studies

An excision wound model was used to illustrate the wound healing ability of the synthesized Ag NPs. During therapy, $ZnO/Ag/Ag_2O_{(CE)}$-treated wounds showed no indication of microbial contamination, hemorrhage, or pus development, whereas the control wounds revealed significant inflammation and bleeding. From day 6 onwards, the $ZnO/Ag/Ag_2O_{(CE)}$-treated group showed distinguished wound closure and decreased wound size, which improved during the remaining days of treatment compared to controls (Supplementary Figure S5).

The $ZnO/Ag/Ag_2O_{(CE)}$-treated wound had approximately 96% closure at the conclusion of the trial, whereas the control wound had approximately 76% closure (Figure 11A). A visual

TABLE 1 Comparative analysis of previous studies.

Compound	Antibacterial study	Antioxidant study (DPPH and reducing power assay)	Anticancer study	Wound healing	Reference
Cellulose/chitosan–Ag/Ag_2O/ZnO (synthetic method)	*E. coli*: 15.0 mm *S. aureus*: 19.6 mm	Not reported	Not reported	Not reported	Peng et al. (2022)
Ag/Ag_2O/ZnO nanocomposites (NCs) via Murusi peel (MP) and Kew peel (KP) (synthetic method)	Not reported	DPPH activity Ag/Ag_2O/ZnO NCs (MP): 78.14 ± 1.04 Ag/Ag_2O/ZnO NCs (KP): 79.18 ± 1.01	Not reported	Not reported	Aththanayaka et al. (2023)
Ag/Ag_2O/ZnO nanocomposite (synthetic method)	7AgZn showed zones of inhibition ranging from 20 mm (*S. aureus* and *E. coli* (1)) to 13 mm (*E. coli*)	Not reported	The cytotoxicity of Ag/Ag_2O/ZnO toward Huh-7 human liver cancer cells was investigated, yielding IC_{50} values of 112.9 μg/mL for samples prepared with 3 mL of $AgNO_3$ (3AgZn) and 313 μg/mL for those prepared with 7 mL (7AgZn)	Not reported	Hezam et al. (2023)
AgO/Ag/ZnO nanocomposite (synthetic method)<	It exhibited a significant ($p > 0.05$) zone of inhibition against *E. coli* and *S. aureus*, followed by *S. typhi*, *B. subtilis*, and *C. albicans* *B. subtilis*: 21.6 ± 0.57	Not reported	AgO/Ag/ZnO nanocomposite has no such toxicity even at a concentration of 100 μg, displaying its non-poisonous property toward normal cells and anticancer potential toward HCT-116 colon cancer cells	Not reported	Ramakrishnegowda et al. (2023)
Ag-ZnO/AgO NPs (synthetic method)	Not reported	Not reported	Not reported	After 21 days, there was an 82.7% reduction in neutrophil activity in wounds treated with Ag-ZnO/AgO NPs compared to the vehicle group	de Moura et al. (2022)
ZnO/Ag/$Ag_2O_{(CE)}$	*B. subtilis*: 25 mm *S. aureus*: 21 mm *E. coli*: 17.5 mm	Reducing power assay: 0.573 absorbance DPPH assay: 86.554% inhibition at 1,000 μg/mL	ZnO/Ag/$Ag_2O_{(CE)}$ showed anticancer activity against the breast cancer cell line MCF7 with an IC_{50} value of 100.23 and 75.27% cell viability	*In vivo* treatment of wounds in an animal model with the ZnO/Ag/$Ag_2O_{(CE)}$ nanocomposite showed approximately 96% closure in 10 days, while the control showed ~50% closure in 10 days	Present research

analysis (Figure 11B) showed that ZnO/Ag/$Ag_2O_{(CE)}$-treated rats had superior wound healing activity than control groups. Previous research has demonstrated the possible influence of AgNPs on wound healing in an animal species and demonstrated that quick healing and improved cosmetic quality appear in a dose-dependent manner. Moreover, AgNPs showed advantages due to their antimicrobial properties, mitigation of wound swelling via decreased lymphocyte and mast cell intrusion, and amendment of fibrogenic cytokines (Tian et al., 2006). Similarly, the impact of AgNPs on dermal stiffness and epidermis re-epithelialization during wound recovery indicated that AgNPs may speed up wound closure (Liu et al., 2010). This characteristic is considered to enhance keratinocyte proliferation and movement.

In addition, AgNPs may promote the differentiation of fibroblasts into myofibroblasts, resulting in wound contraction (Gunasekaran et al., 2011). Zinc oxide is valuable in wound dressings because of its capability to protect against bacteria (Shu et al., 2023). The enhanced wound healing efficacy results primarily from the synergistic antimicrobial effects of Ag and Zn, leading to a reduction in inflammation. This not only prevents additional infections in the wound but also accelerates the epithelialization process by creating a favorable healing environment (Kantipudi et al., 2018).

Peng, Y. et al. (2022) demonstrated the preparation of cellulose/chitosan/Ag/Ag_2O/ZnO nanocomposites through synthetic methods, evaluating their efficacy against *E. coli* and *S. aureus* bacterial strains (Peng et al., 2022). Aththanayaka, S. et al. (2023) outlined a synthetic approach for synthesizing Ag/Ag_2O/ZnO nanocomposites utilizing Murusi peel and Kew peel, showcasing promising antioxidant activity through DPPH radical scavenging assays (Aththanayaka et al., 2023). Hezam,

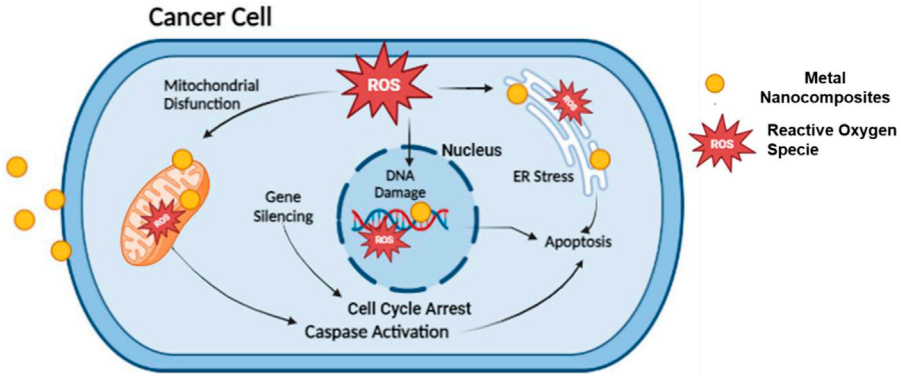

FIGURE 10
Proposed anticancer activity mechanism of the ZnO/Ag/Ag_2O nanocomposite.

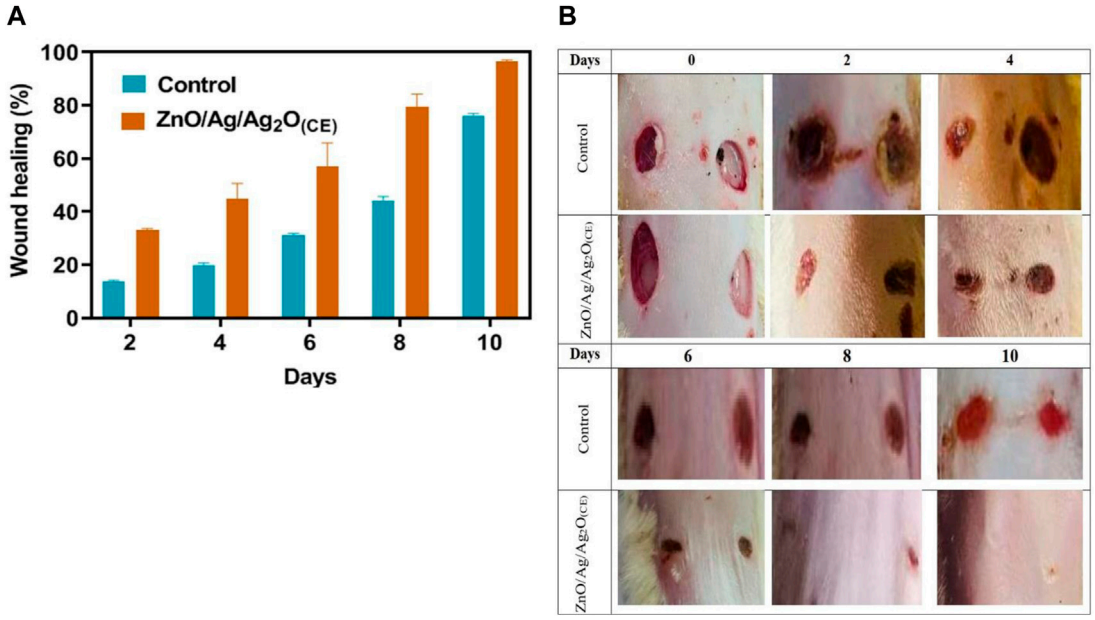

FIGURE 11
Quantitative **(A)** and visual **(B)** analysis of wound healing in rats.

A. et al. (2023) attributed the antibacterial activity of Ag, ZnO, and Ag_2O to intrinsic properties while also investigating the cytotoxicity of Ag/Ag_2O/ZnO on Huh-7 human liver cancer cells, yielding IC_{50} values of 112.9 and 313 μg/mL for samples prepared using 3 mL (3AgZn) and 7 mL $AgNO_3$ (7AgZn), respectively (Hezam et al., 2023). Ramakrishnegowda, D. H. et al. (2023) reported potent antibacterial activity against *E. coli*, *S. aureus*, and *B. subtilis*, with higher efficacy observed against *Salmonella typhi*. Additionally, AgO/Ag/ZnO exhibited superior inhibition of *Candida albicans* compared to the standard, along with potent anticancer activity against HCT-116 cell lines (IC_{50} value: 16.61 μg/mL) (Ramakrishnegowda et al., 2023). de Moura et al. (2022) conducted wound healing analysis, revealing an 82.7% reduction in neutrophil activity after 21 days in wounds treated with Ag-ZnO/AgO nanoparticles compared to the vehicle group (de Moura et al., 2022). A comparative literature review have also been summarized in Table 1 for the reader's interest. Building on these findings, our present research on the ZnO/Ag/$Ag_2O_{(CE)}$ nanocomposite comprehensively examines its antibacterial activity, showcasing the highest zone of inhibition against *B. subtilis*, along with their antioxidant, anticancer, and wound healing activities, demonstrating 96% healing within 10 days.

4 Conclusion

In conclusion, an ecofriendly method was used to fabricate stable $ZnO_{(CE)}$ NPs and Ag/$Ag_2O_{(CE)}$ and ZnO/Ag/$Ag_2O_{CE)}$ nanocomposites using *S. hispanica* L. (commonly known as chia

seeds) extract without any special capping agent. The synthesized nanocomposites were characterized by UV–visible, FTIR, SEM, and XRD techniques. The XRD analysis revealed that the crystallite sizes of $ZnO_{(CE)}$ NPs and $Ag/Ag_2O_{(CE)}$ and $ZnO/Ag/Ag_2O_{(CE)}$ nanocomposites were 16.15 nm, 46.6 nm, and 22.42 nm, respectively. The SEM analysis showed that $Ag/Ag_2O_{(CE)}$ had hetero-structure particles, $ZnO_{(CE)}$ had agglomerated nanoparticles, and $ZnO/Ag/Ag_2O_{(CE)}$ exhibited a spherical particle-like morphology of the composite. $ZnO_{(CE)}$ NPs and $Ag/Ag_2O_{(CE)}$ and $ZnO/Ag/Ag_2O_{(CE)}$ nanocomposites exhibited good antibacterial activity against *S. aureus, E. coli*, and *B. subtilis*. The resistance of these nanoparticles and nanocomposites to *B. subtilis* bacterial strains was 17 mm, 16 mm, and 25.3 mm, respectively. The highest antioxidant activity, including reducing power activity and DPPH radical scavenging activity, was depicted by $ZnO/Ag/Ag_2O_{(CE)}$, while the lowest activity was shown by $Ag/Ag_2O_{(CE)}$. $ZnO/Ag/Ag_2O_{(CE)}$ toward the MCF7 cancer cell line yielded the highest *in vitro* anticancer activity, i.e., 75.27% inhibition at a sample concentration of 100 µg/mL. Finally, the *in vivo* treatment of wounds in an animal model with the $ZnO/Ag/Ag_2O_{(CE)}$ nanocomposite showed approximately 96% closure in 10 days, while the control showed ~50% closure in 10 days. These findings emphasize the significant role of ecofriendly fabricated multifunctional $ZnO/Ag/Ag_2O_{(CE)}$ nanocomposites in cancer inhibition and wound healing processes.

Data availability statement

The original contributions presented in the study are included in the article/Supplementary Material, further inquiries can be directed to the corresponding authors.

Ethics statement

The animal study was approved by the Animal Ethics Committee, Government College University Faisalabad. The study was conducted in accordance with the local legislation and institutional requirements.

Author contributions

AR: investigation, writing–original draft, funding acquisition, validation, and visualization. FA: data curation, formal analysis, software, and writing–review and editing. MJ: data curation, formal analysis, writing–review and editing, and resources. SN: conceptualization, methodology, project administration, and writing–original draft. SH: conceptualization, methodology, visualization, and writing–original draft. HA: data curation, software, and writing–review and editing. MN: data curation, formal analysis, and writing–review and editing. ZA: formal analysis, resources, and writing–review and editing. AA: data curation, funding acquisition, and writing–review and editing. MM: data curation, software, validation, and writing–review and editing. AM: data curation, validation, and writing–review and editing. MB: data curation, formal analysis, validation, funding acquisition, visualization, software, writing–review and editing. AA: data curation, conceptualization, formal analysis, validation, funding acquisition, visualization, writing–review and editing.

Funding

The author(s) declare that financial support was received for the research, authorship, and/or publication of this article. The Princess Nourah bint Abdulrahman University Researchers Supporting (project number: PNURSP2024R224), Princess Nourah bint Abdulrahman University, Riyadh, Saudi Arabia. Research Project under grant number RGP2/454/44; Deanship of Scientific Research at King Khalid University.

Acknowledgments

The authors acknowledge the Princess Nourah bint Abdulrahman University Researchers Supporting (project number: PNURSP2024R224), Princess Nourah bint Abdulrahman University, Riyadh, Saudi Arabia. The authors acknowledge the Deanship of Scientific Research at King Khalid University for funding this work through the Research Project under grant number RGP2/454/44. The authors acknowledge the Department of Chemistry and Department of Pharmaceutics, Government College University Faisalabad (GCUF), and COMSATS University Islamabad, Lahore Campus, Lahore, Pakistan, for providing the experimental support to undertake this research.

Conflict of interest

The authors declare that the research was conducted in the absence of any commercial or financial relationships that could be construed as a potential conflict of interest.

Publisher's note

Supplementary material

The Supplementary Material for this article can be found online at: https://www.frontiersin.org/articles/10.3389/fchem.2024.1405385/full#supplementary-material

References

Al-Shmgani, H. S., Mohammed, W. H., Sulaiman, G. M., and Saadoon, A. H. (2016). Biosynthesis of silver nanoparticles from catharanthus roseus leaf extract and assessing their antioxidant, antimicrobial, and wound-healing activities. *Artif. Cells Nanomedicine Biotechnol.* 45 (6), 1234–1240. doi:10.1080/21691401.2016.1220950

Althubiti, N. A., Taha, T. A., Azab, A. A., and Abdelhamid, H. N. (2023). ZnO-based nanocomposites for hydrogen generation via hydrolysis of borohydride. *J. Sol-Gel Sci. Technol.* 106 (3), 837–846. doi:10.1007/s10971-023-06099-6

Amir, M., Sharma, R., Mishra, V., Wazed Ali, S., and Khan, G. S. (2022). Polishing performance of magnetic nanocomposites based nanoabrasive. *Mater. Today Proc.* 56, 549–554. doi:10.1016/j.matpr.2022.02.276

Aththanayaka, S., Thiripuranathar, G., and Ekanayake, S. (2023). Microwave-assisted phytogenic Ag/Ag2O/ZnO nanocomposite as a replacement of Ag/Ag2O and ZnO nanoparticles: a comparative antioxidant study. *Surfaces Interfaces* 43, 103547. doi:10.1016/j.surfin.2023.103547

Awan, S. S., Khan, R. T., Mehmood, A., Hafeez, M., Abass, S. R., Nazir, M., et al. (2023). Ailanthus altissima leaf extract mediated green production of zinc oxide (ZnO) nanoparticles for antibacterial and antioxidant activity. *Saudi J. Biol. Sci.* 30 (1), 103487. doi:10.1016/j.sjbs.2022.103487

Barwant, M., Ugale, Y., Ghotekar, S., Basnet, P., Nguyen, V., Pansambal, S., et al. (2022). Eco-friendly synthesis and characterizations of Ag/AgO/Ag2O nanoparticles using leaf extracts of solanum elaeagnifolium for antioxidant, anticancer, and DNA cleavage activities. *Chem. Pap.* 76 (7), 4309–4321. doi:10.1007/s11696-022-02178-0

Batool, M., Khurshid, S., Qureshi, Z., and Daoush, W. M. (2020). Adsorption, antimicrobial and wound healing activities of biosynthesised zinc oxide nanoparticles. *Chem. Pap.* 75 (3), 893–907. doi:10.1007/s11696-020-01343-7

Bilal, B., Niazi, R., Nadeem, S., Farid, M. A., Nazir, M. S., Akhter, T., et al. (2022). Fabrication of guided tissue regeneration membrane using lignin-mediated ZnO nanoparticles in biopolymer matrix for antimicrobial activity. *Front. Chem.* 10, 837858. doi:10.3389/fchem.2022.837858

Borzęcka, W., Pereira, P. M. R., Fernandes, R., Trindade, T., Torres, T., and Tomé, J. P. C. (2022). Spherical and rod shaped mesoporous silica nanoparticles for cancer-targeted and photosensitizer delivery in photodynamic therapy. *J. Mater Chem. B* 10, 3248–3259. doi:10.1039/d1tb02299g

Chen, Q., Jiang, H., Ye, H., Li, J., and Huang, J. (2014). Preparation, antibacterial, and antioxidant activities of silver/chitosan composites. *J. Carbohydr. Chem.* 33 (6), 298–312. doi:10.1080/07328303.2014.931962

Cushen, M., Kerry, J., Morris, M., Cruz-Romero, M., and Cummins, E. (2014). Evaluation and simulation of silver and copper nanoparticle migration from polyethylene nanocomposites to food and an associated exposure assessment. *J. Agric. Food Chem.* 62, 1403–1411. doi:10.1021/jf404038y

de Moura, F. B. R., Ferreira, B. A., Muniz, E. H., Justino, A. B., Silva, A. G., De Azambuja Ribeiro, R. I. M., et al. (2022). Antioxidant, anti-inflammatory, and wound healing effects of topical silver-doped zinc oxide and silver oxide nanocomposites. *Int. J. Pharm.* 617, 121620. doi:10.1016/j.ijpharm.2022.121620

Ding, W., Zhao, L., Yan, H., Wang, X., Liu, X., Zhang, X., et al. (2019). Bovine serum albumin assisted synthesis of Ag/Ag2O/ZnO photocatalyst with enhanced photocatalytic activity under visible light. *Colloids Surfaces A Physicochem. Eng. Aspects* 568, 131–140. doi:10.1016/j.colsurfa.2019.02.015

Elyamny, S., Eltarahony, M., Abu-Serie, M. M., Nabil, M., and Kashyout, A. E.-H. B. (2021). One-pot fabrication of Ag @Ag2O core–shell nanostructures for biosafe antimicrobial and antibiofilm applications. *Sci. Rep.* 11 (1), 22543. doi:10.1038/s41598-021-01687-4

Ganguli, P., and Chaudhuri, S. (2021). Nanomaterials in antimicrobial paints and coatings to prevent biodegradation of man-made surfaces: a review. *Mater. Today Proc.* 45, 3769–3777. doi:10.1016/j.matpr.2021.01.275

Gülçın, İ., Oktay, M., Kıreçcı, E., and Küfrevioğlu, Ö. İ. (2003). Screening of antioxidant and antimicrobial activities of anise (pimpinella anisum L.) seed extracts. *Food Chem.* 83 (3), 371–382. doi:10.1016/s0308-8146(03)00098-0

Gunasekaran, T., Nigusse, T., and Dhanaraju, M. D. (2011). Silver nanoparticles as real topical bullets for wound healing. *J. Am. Coll. Clin. Wound Specialists* 3 (4), 82–96. doi:10.1016/j.jcws.2012.05.001

Gupta, A., Mumtaz, S., Li, C. H., Hussain, I., and Rotello, V. M. (2019). Combatting antibiotic-resistant bacteria using nanomaterials. *Chem. Soc. Rev.* 48, 415–427. doi:10.1039/c7cs00748e

Haleem, A., Javaid, M., Singh, R. P., Rab, S., and Suman, R. (2023). Applications of nanotechnology in medical field: a brief review. *Glob. Health J.* 7, 70–77. doi:10.1016/j.glohj.2023.02.008

Hashem, A. H., and El-Sayyad, G. S. (2023). Antimicrobial and anticancer activities of biosynthesized bimetallic silver-zinc oxide nanoparticles (Ag-ZnO NPs) using pomegranate peel extract. *Biomass Convers. Biorefinery*. doi:10.1007/s13399-023-04126-8

Hernández-Morales, L., Espinoza-Gómez, H., Flores-López, L. Z., Sotelo-Barrera, E. L., Núñez-Rivera, A., Cadena-Nava, R. D., et al. (2019). Study of the green synthesis of silver nanoparticles using a natural extract of dark or white Salvia hispanica L. seeds and their antibacterial application. *Appl. Surf. Sci.* 489, 952–961. doi:10.1016/j.apsusc.2019.06.031

Hezam, A., Abutaha, N., Almekhlafi, F. A., Saeed, A. M. N., Abishad, P., and Wadaan, M. A. (2023). Smart plasmonic Ag/Ag2O/ZnO nanocomposite with promising photothermal and photodynamic antibacterial activity under 600 nm visible light illumination. *J. Photochem. Photobiol. A Chem.* 435, 114322. doi:10.1016/j.jphotochem.2022.114322

Hosseini, S. M., Sarsari, I. A., Kameli, P., and Salamati, H. (2015). Effect of Ag doping on structural, optical, and photocatalytic properties of ZnO nanoparticles. *J. Alloys Compd.* 640, 408–415. doi:10.1016/j.jallcom.2015.03.136

Jaiswal, K. K., Banerjee, I., Dutta, S., Verma, R., Gunti, L., Awasthi, S., et al. (2022). Microwave-assisted polycrystalline Ag/AgO/AgCl nanocomposites synthesis using banana corm (rhizome of musa sp.) extract: characterization and antimicrobial studies. *J. Industrial Eng. Chem.* 107, 145–154. doi:10.1016/j.jiec.2021.11.041

Järbrink, K., Ni, G., Sönnergren, H., Schmidtchen, A., Pang, C., Bajpai, R., et al. (2017). The humanistic and economic burden of chronic wounds: a protocol for a systematic review. *Syst. Rev.* 6, 15. doi:10.1186/s13643-016-0400-8

Kantipudi, S., Sunkara, J. R., Rallabhandi, M., Thonangi, C. V., Cholla, R. D., Kollu, P., et al. (2018). Enhanced wound healing activity of Ag–ZnO composite NPs in wistar albino rats. *Iet Nanobiotechnology* 12 (4), 473–478. doi:10.1049/iet-nbt.2017.0087

Karthick, A. S., Nisha, S., and Nallathambi, A. (2012). A review on methods, application and properties of immobilized enzyme chemical science review and letters A review on methods, application and properties of immobilized Enzyme.2012 *correspondence. *Che Sci. Rev. Lett.* 1 (3).

Laouini, S. E., Bouafia, A., Солдатов, A. B., Algarni, H., Tedjani, M. L., Ali, G. a. M., et al. (2021). Green synthesized of Ag/Ag2O nanoparticles using aqueous leaves extracts of Phoenix dactylifera L. And their azo dye photodegradation. *Membranes* 11 (7), 468. doi:10.3390/membranes11070468

Lawrence, R. (2015). *Green synthesis and Anti-bacterial activity of Silver Oxide nanoparticles prepared from Pinuslongifolia leaves extract*. Natural Product Chemistry View project working on essential oil View project.

Li, L., Jing, D., Deng, H., Liu, Z., and Li, X. (2010). Preparation, characterization and antimicrobial activities of chitosan/Ag/ZnO blend films. *Chem. Eng. J.* 160 (1), 378–382. doi:10.1016/j.cej.2010.03.051

Li, S., Renick, P., Senkowsky, J., Nair, A., and Tang, L. (2021). Diagnostics for wound infections. *Adv. Wound Care (New Rochelle)* 10, 317–327. doi:10.1089/wound.2019.1103

Liu, X., Lee, P., Ho, C. S., Lui, V. C. H., Chen, Y., Che, C., et al. (2010). Silver nanoparticles mediate differential responses in keratinocytes and fibroblasts during skin wound healing. *ChemMedChem* 5 (3), 468–475. doi:10.1002/cmdc.200900502

Liu, Y., and Kim, H. I. (2012). Characterization and antibacterial properties of genipin-crosslinked chitosan/poly(ethylene glycol)/ZnO/Ag nanocomposites. *Carbohydr. Polym.* 89 (1), 111–116. doi:10.1016/j.carbpol.2012.02.058

Mahmoudi, A., Tavakoly Sany, S. B., Ahari Salmasi, M., Bakhshi, A., Bustan, A., Heydari, S., et al. (2023). Application of nanotechnology in air purifiers as a viable approach to protect against Corona virus. *IET Nanobiotechnol* 17, 289–301. doi:10.1049/nbt2.12132

Malik, S., Singh, J., Goyat, R., Saharan, Y., Chaudhry, V., Umar, A., et al. (2023). Nanomaterials-based biosensor and their applications: a review. *Heliyon* 9, e19929. doi:10.1016/j.heliyon.2023.e19929

Malone, M., Bjarnsholt, T., McBain, A. J., James, G. A., Stoodley, P., Leaper, D., et al. (2017). The prevalence of biofilms in chronic wounds: a systematic review and meta-analysis of published data. *J. Wound Care* 26, 20–25. doi:10.12968/jowc.2017.26.1.20

Mohan, A. C., and Renjanadevi, B. (2016). Preparation of zinc oxide nanoparticles and its characterization using scanning electron microscopy (SEM) and X-ray diffraction(XRD). *Procedia Technol.* 24, 761–766. doi:10.1016/j.protcy.2016.05.078

Nandhini, J., Karthikeyan, E., and Rajeshkumar, S. (2024). Nanomaterials for wound healing: current status and futuristic frontier. *Biomed. Technol.* 6, 26–45. doi:10.1016/j.bmt.2023.10.001

Narayan, K. M. V., Williams, D., Gregg, E. W., and Cowie, C. C. (2010). *Diabetes public health: from data to policy*. Oxford University Press.

Naseem, T., and Durrani, T. (2021). The role of some important metal oxide nanoparticles for wastewater and antibacterial applications: a review. *Environ. Chem. Ecotoxicol.* 3, 59–75. doi:10.1016/j.enceco.2020.12.001

Nirmala, M. J., Kizhuveetil, U., Johnson, A., G, B., Nagarajan, R., and Muthuvijayan, V. (2023). Cancer nanomedicine: a review of nano-therapeutics and challenges ahead. *RSC Adv.* 13, 8606–8629. doi:10.1039/d2ra07863e

Nussbaum, S. R., Carter, M. J., Fife, C. E., DaVanzo, J., Haught, R., Nusgart, M., et al. (2018). An economic evaluation of the impact, cost, and medicare policy implications of chronic nonhealing wounds. *Value Health* 21, 27–32. doi:10.1016/j.jval.2017.07.007

Pandi, V. S., Anusuya, M., Dagar, A., and Annu Dagar, (2023). Synthesis and characterization of ZnO, ZnO doped Ag_2O nanoparticles and its photocatalytic activity. *Sci. Temper* 14 (03), 827–833. doi:10.58414/scientifictemper.2023.14.3.41

Patra, S., Mishra, S., Parhi, B., Mishra, H., and Swain, S. K. (2023). Role of transition metal nanocomposites in organic reactions: a state of art as an alternative to conventional catalysts. *Results Chem.* 6, 101172. doi:10.1016/j.rechem.2023.101172

Peng, Y., Zhou, H., Wu, Y., Ma, Z., Zhang, R., Tu, H., et al. (2022). A new strategy to construct cellulose-chitosan films supporting Ag/Ag2O/ZnO heterostructures for high photocatalytic and antibacterial performance. *J. Colloid Interface Sci.* 609, 188–199. doi:10.1016/j.jcis.2021.11.155

Rajendran, N. K., Kumar, S. S. D., Houreld, N. N., and Abrahamse, H. (2018). A review on nanoparticle based treatment for wound healing. *J. Drug Deliv. Sci. Technol.* 44, 421–430. doi:10.1016/j.jddst.2018.01.009

Ramakrishnegowda, D. H., Swamy, C. K., Kumar, B. A., Rangappa, S., Rangappa, K. S., and Shivanna, S. (2023). Ag mediated plasmonic AgO/ZnO composite and its pharmaceutical relevance. *Mater. Sci. Eng. B* 292, 116437. doi:10.1016/j.mseb.2023.116437

Reyes-Caudillo, E., Tecante, A., and Valdivia-López, M. A. (2008). Dietary fibre content and antioxidant activity of phenolic compounds present in Mexican chia (Salvia hispanica L.) seeds. *Food Chem.* 107, 656–663. doi:10.1016/j.foodchem.2007.08.062

Roshani, M., Rezaian-Isfahni, A., Lotfalizadeh, M. H., Khassafi, N., Abadi, M. H. J. N., and Nejati, M. J. C. C. I. (2023). Metal nanoparticles as a potential technique for the diagnosis and treatment of gastrointestinal cancer: a comprehensive review. *a Compr. Rev.* 23 (1), 280. doi:10.1186/s12935-023-03115-1

Senapati, S., Mahanta, A. K., Kumar, S., and Maiti, P. (2018). Controlled drug delivery vehicles for cancer treatment and their performance. *Signal Transduct. Target Ther.* 3, 7. doi:10.1038/s41392-017-0004-3

Sharma, A., Shambhwani, D., Pandey, S., Singh, J., Lalhlenmawia, H., Kumarasamy, M., et al. (2023). Advances in lung cancer treatment using nanomedicines. *ACS Omega* 8, 10–41. doi:10.1021/acsomega.2c04078

Shu, G., Xu, D., Xie, S., Chang, L., Liu, X., Jian, Y., et al. (2023). The antioxidant, antibacterial, and infected wound healing effects of ZnO quantum dots-chitosan biocomposite. *Appl. Surf. Sci.* 611, 155727. doi:10.1016/j.apsusc.2022.155727

Sobhani-Nasab, A., and Behpour, M. (2015). Synthesis and characterization of AgO nanostructures by precipitation method and its photocatalyst application. *J. Mater. Sci. Mater. Electron.* 27 (2), 1191–1196. doi:10.1007/s10854-015-3873-7

Solanki, P. R., Kumar, A., Singh, R. P., Singh, J., and Singh, K. R. (2023). *Nanotechnological aspects for next-generation wound management*. Elsevier.

Soni, N., and Dhiman, R. C. (2017). Phytochemical, anti-oxidant, larvicidal, and antimicrobial activities of Castor (ricinus communis) synthesized silver nanoparticles. *Chin. Herb. Med.* 9 (3), 289–294. doi:10.1016/s1674-6384(17)60106-0

Sophia, P. J., Balaji, D., Peters, T., Chander, D. S., Rishaban, S. V., Shanthi, P. V., et al. (2020). Solar induced photocatalytic degradation of methylene blue by CDS/AG2O nanocomposites. *ChemistrySelect* 5 (14), 4125–4135. doi:10.1002/slct.202000475

Sorbiun, M., Mehr, E. S., Ramazani, A., and Fardood, S. T. (2018). Green synthesis of zinc oxide and copper oxide nanoparticles using aqueous extract of oak fruit hull (JAFT) and comparing their photocatalytic degradation of basic violet 3. *Int. J. Environ. Res.* 12 (1), 29–37. doi:10.1007/s41742-018-0064-4

Swanson, T., Keast, D., Cooper, R., Black, J., Angel, D., Schultz, G., et al. (2015). Ten top tips: identification of wound infection in a chronic wound. *Wounds Int.* 6 (2), 22–27.

Thatikayala, D., Banothu, V., Kim, J.-S., Shin, D. B., Vijayalakshmi, S., and Park, J. (2020). Enhanced photocatalytic and antibacterial activity of ZnO/Ag nanostructure synthesized by Tamarindus indica pulp extract. *J. Mater. Sci. Mater. Electron.* 31 (7), 5324–5335. doi:10.1007/s10854-020-03093-4

Tian, J., Wong, K. K., Ho, C. M., Lok, C. N., Yu, W., Ming, C., et al. (2006). Topical delivery of silver nanoparticles promotes wound healing. *ChemMedChem* 2 (1), 129–136. doi:10.1002/cmdc.200600171

Umukoro, E. H., Peleyeju, M. G., Ngila, J. C., and Arotiba, O. A. (2016). Photocatalytic degradation of acid blue 74 in water using Ag–Ag 2 O–zno nanostuctures anchored on graphene oxide. *Solid State Sci.* 51, 66–73. doi:10.1016/j.solidstatesciences.2015.11.015

Włodarczyk, R., and Kwarciak-Kozłowska, A. (2021). Nanoparticles from the cosmetics and medical industries in legal and environmental aspects. *Sustainability* 13, 5805. doi:10.3390/su13115805

Yang, H., Tian, J., Li, T., and Cui, H. (2016). Synthesis of novel Ag/Ag2O heterostructures with solar full spectrum (UV, visible and near-infrared) light-driven photocatalytic activity and enhanced photoelectrochemical performance. *Catal. Commun.* 87, 82–85. doi:10.1016/j.catcom.2016.09.013

Ying, S., Guan, Z., Ofoegbu, P. C., Clubb, P., Rico, C., He, F., et al. (2022). Green synthesis of nanoparticles: current developments and limitations. *Environ. Technol. Innovation* 26, 102336. doi:10.1016/j.eti.2022.102336

Zafar, S., Hasnain, Z., Aslam, N., Mumtaz, S., Jaafar, H. Z. E., Wahab, P. E. M., et al. (2021). Impact of Zn nanoparticles synthesized via green and chemical approach on okra (abelmoschus esculentus L.) growth under salt stress. *Sustainability* 13 (7), 3694. doi:10.3390/su13073694